ORAL REFERENCE: ICF100114OR

MEASURING CRACK TIP DEFORMATION IN NANOSCOPIC RESOLUTION

Y. M. Xing[1,2] and W. Yang[1]

[1] FML, Department of Engineering Mechanics, University of Tsinghua, Beijing, 100084, China
[2]Department of Basic Science, Inner Mongolia Polytechnic University, Hohhot, 010062, China

ABSTRACT

Interference of HREM image of deformed crystal with unidirectional reference gratings leads to direct measurement of displacements and strains of nanoscopic resolution. The fringe contrast is enhanced by an optical filtering technique. Using the HREM moiré method, we measure the near tip nanoscopic deformation on the {111} plane of single crystal silicon with a loaded quasi-cleavage crack running in the [110] direction. The measured strain distribution ahead of the crack tip agrees with the linear elastic fracture mechanics prediction up to 10nm from the crack tip. Dislocations of Peierls type are detected and they extend from the crack tip over a length of hundreds of Burgers vectors.

KEYWORDS

Crack tip, nanoscopic deformation, measurement, dislocation,

INTRODUCTION

Dislocation nucleation from a crack tip underlies the mechanism of brittle versus ductile transition [1]. In a pioneering work for the competition between cleavage crack growth and dislocation emission from a crack tip, Rice and Thomson [2] performed an activation analysis in which the total energy change due to the formation of a dislocation half loop at the crack tip was calculated as a function of the loop radius and the dislocation core cut-off radius. Later on, the concept of Peierls-dislocation [3] was introduced to remove the uncertainty of the dislocation core cut-off radius and to formulate the concept of unstable stacking energy [4]. The competition between cleavage and dislocation emission can be revealed in microscopic details by testing single crystals. With known dopant level and sharp transition temperature, silicon or iron-silicon crystal is a frequent choice for the observation of dislocation emission from a crack tip [5].

Optical techniques have been used extensively in the direct determination of crack tip deformation fields. Current moiré technology, from moiré interferometry to electron beam moiré, has a grating frequency

from 1200 to 10000 lines/mm [6]. Recently, the authors proposed the HREM-moiré method [7]. The fundamental limitation on a perfect crystal is the constancy of its lattice spacing with respect to thermal vibration at room temperature. Silicon single crystal has a lattice structure with a period of 0.304nm, which represents a grating with a frequency of 3289474 lines/mm. Such a high-frequency grating allows measurement with atom-size sensitivity and nanoscopic resolution. When the specimen is loaded, the deformation alters the spacing of lattice and may cause dislocation emission. The changes in the microstructure are recorded by the HREM image. The principle of moiré formation is the same as the one in geometric moiré. The HREM image of the crystal lattice acts as a specimen grating. The optical grating with standard spacing acts as a reference grating. Under a proper magnification, the specimen grating is superimposed onto the reference grating and moiré patterns emerge that reveal displacements, strains and lattice defects.

Since the crystal lattice is commonly packed in non-orthogonal array, the uni-directional reference grating, rather than the cross-line gratings in the geometric moiré method, is used. The moiré fringes represent the displacement components normal to the reference-grating lines. One can align the reference-grating lines exactly with the lattice lines in *y*-direction to measure the displacement component u_x, then rotates the reference-grating an angle θ to another set of lattice lines to obtain the displacement component u_r. If there is no mismatch between the reference grating and the non-deformed crystal lattice under amplification, the displacements u_x and u_r can be expressed by

$$u_x = \frac{N_x p}{M}, \quad u_r = \frac{N_r p}{M} \quad (N_x、N_r=0，1，2\bullet\bullet\bullet) \qquad (1)$$

where p denotes the reference-grating pitch, M the magnification of TEM, and N_x and N_r the fringe orders in the x and r directions. The in-plane strain components are determined by

$$\varepsilon_x = \frac{p}{Mf_{xx}}, \quad \varepsilon_r = \frac{p}{Mf_{rr}}, \quad \gamma_{xy} = \frac{p}{Mf_{xy}} + \frac{p}{Mf_{rx}}\sin\theta \qquad (2)$$

The values f_{xx} , f_{rr}, f_{rx}, and f_{xy} are the intervals between adjacent fringes, the first index represents the normal of the reference grating and the second index the measuring direction of the fringe interval. For a valid measurement, the specimens must be thin enough so that the weak-phase-body hypothesis is valid, and the adjustment of object glass of TEM must satisfy Scherzer's under-focus condition [8]. One can modify the reference grating by slight rotation mismatch (characterized by a rigid body rotation angle α) and/or stretching mismatch (characterized by a constant strain ε) to obtain subtle features of the deformation field.

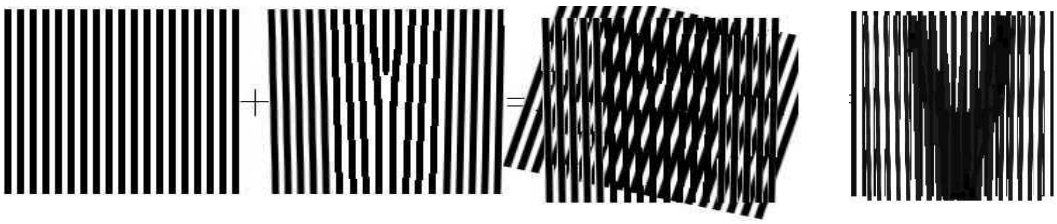

Angular mismatch moiré Parallel moiré

Figure 1 Illustration of moiré patterns for dislocation

Moiré fringes can also be used to measure the lattice slip δ and to identifythe dislocation. Dislocations occur at the places where fringes join or drop. The joining fringes are formed by aligning the reference-grating lines parallel to the specimen-grating lines; and dropped ones by placing the reference grating lines in an inclined angle with the specimen grating, as simulated in Figure 1. Even the incomplete or Peierls dislocation can be identified by the shearing of moire fringes. Moiré patterns with

these signatures are easy to be identified from the HREM image and reference grating interference.

The fringes produced by direct superposition of HREM image of crystal lattices and reference grating are hardly visible. But they can be transformed into fringes of high contrast by an optical filtering process as illustrated in Figure 2. The light that passes through the grating structure is diffracted into several diffraction orders, while the light that passes through the gray continuous-tone areas does not diffract. The field lens converges the transmitted beams to separate points in its focal plane, corresponding to diffraction orders from the striped areas. The light from the continuous-tone areas converges to point 0. The camera only admits light of one nonzero diffraction order, the image on the camera screen is bright at all points corresponding to striped areas, and dark elsewhere. Both coherent and non-coherent lights can be chosen as the light source in the filtering apparatus. We use laser here to obtain higher fringe contrast and resolution, at the risk of speckle noise. A Panasonic WV-BP310/G CCD video camera connected to a microcomputer collects all images.

Initial fringes may occur due to either initial lattice defects or the mismatch between lattice image and reference grating. We recorded the specimen-lattice images before and after loading. The actual results are delivered by subtracting the initial data from the final ones. A reference area is selected. It should be free of defects, unloaded or with diminishing stress. The fringes in that area characterize the mismatch between the magnified lattice spacing and the reference grating. The mismatch fringes are then subtracted from the final results.

The testing samples were cut from a Si sheet in the primary cleavage plane {111} so that the lattice image can be easily recorded. The loading device and the specimen geometry are shown in Figure 3. The specimen was ground mechanically into a sheet of diameter d = 2mm and thickness h = 30 μm. The central area for the TEM analysis was thinned out by ionic bombardment till punching. A pre-compressed copper ring of diameter 2mm and thickness 0.4mm was glued on one side of the specimen, with the compression axis normal to the [110] direction. When the glue solidified, the copper ring was unloaded to exert tensile force onto the specimen. That process resembles displacement-controlled loading and creates a stable and atomistically sharp crack in the most cleavable direction of [110]. The crack arrests after propagating a limited distance.

A transmission electronic microscope (JEM-200cx) was used to take the lattice image and the moiré fringes were produced by the method mentioned above. The magnification is 200,000 times. The magnified lattice lines in [110] direction have a frequency of about 16 lines/mm. Accordingly, adjacent fringes roughly represent the difference of one Burgers vector in the normal displacements. Figure 4(a) is the fringe pattern without rigid-rotation mismatch. The nano-crack approximately lies in the horizontal direction. Symbols D and A label the locations of the crack tip before and after loading. The discontinuity of the out-of-plane displacement along the crack makes the focusing on both sides of the crack difficult, so we only present the fringe pattern above the crack. The fringe pattern represents the contour map of the displacement in y-direction, though includes initial mismatch fringes between lattice image and reference grating.

Direct measurement of the strain distribution ahead of a crack tip is instrumental to understand the microscopic failure mechanism of brittle materials. In the present test, the distribution of strain in y-direction along the line AX was obtained from the fringe pattern in Figure 4(a). Up to now all crack tip strain measurements can only reach a resolution of about 0.1micron [9]. The measurements (with the initial fringes subtracted) shown by the square dots in Figure 5, however, provides data points as close as 4nm from the crack tip. The measured strain distribution was compared to the solid curve plotted under the linear elastic fracture mechanics (LEFM) prediction $\varepsilon_y = K(1-\nu)/(E\sqrt{2\pi x})$ under the plane stress case, where $K \approx 1.21\text{MPa}\sqrt{\text{m}}$ is the correlated mode I stress intensity factor. A Young's modulus of

107GPa and a Poisson's ratio of 0.3 are used for silicon in that correlation. The HREM-moiré measurements on strain agree perfectly with the LEFM prediction up to 10nm from the crack tip. Within the 10nm range, the measured strain is somewhat lower than the LEFM prediction. The strain at the crack tip may reach 5%, indicting an in-plane equal-biaxial stress as high as 7.6GPa.

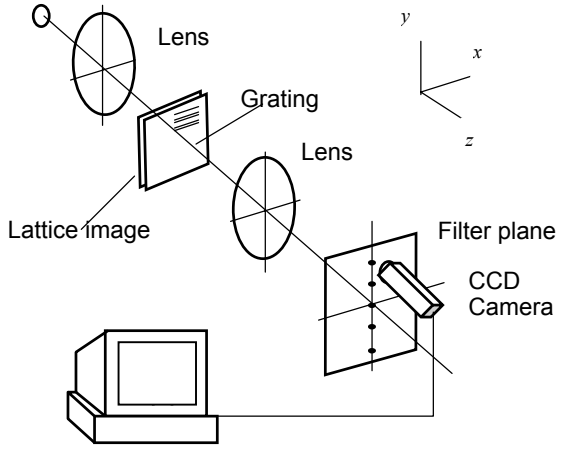

Figure 2 Optical filtering apparatus

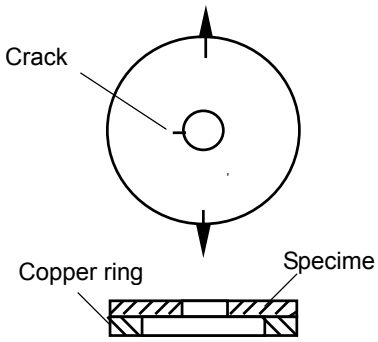

Figure 3 Specimen and loading device

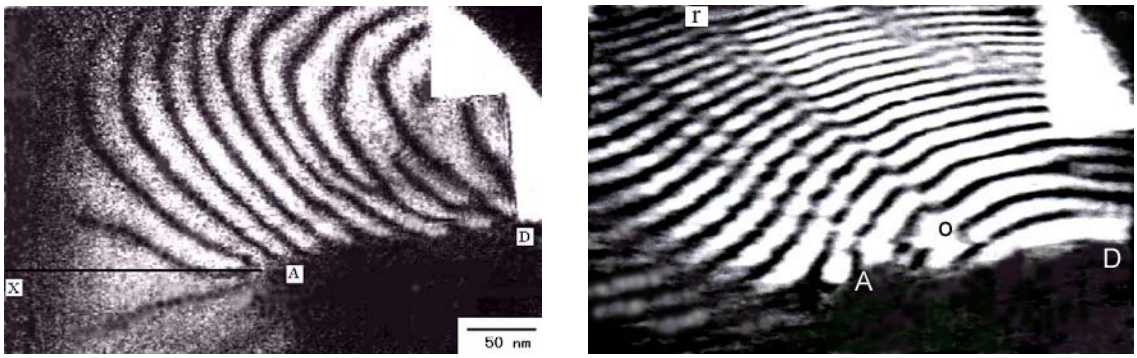

(a) (b)

Figure 4 Moiré fringe patterns near a crack tip: (a) without rigid-body-rotation mismatch, and (b) with rigid-body-rotation (α=0.011 rad) and constant strain ($\varepsilon = -0.035$) mismatch.

Figure 4(b) shows the moiré fringes that were deliberately taken to reveal dislocation emission from the crack tip. A slightly coarser reference grating was designed to get denser moiré fringes, and the reference grating was rotated slightly to resolve the kinking of moiré fringes across the dislocation planes. Through calibration at the location remote from the crack tip, we found those operations rotate the reference grating by $\alpha = 0.011$ radians and superpose a uniform strain of $\varepsilon = -0.035$ in the y direction. The fringes join or drop at a few places near the crack line. The amount of dislocation emissions is less than the previous observation [6]. The reasons may be listed as follows: (1) the current test was carried out in single crystal silicon at room temperature ($T = 24.5^{\circ}\mathrm{C}$); (2) the crack extends in the most cleavable plane of [110] while the dislocations emit from the non-primary glide plane; and (3) the deformation field for closely packed dislocations or dislocation dipoles are hardly resolvable at nanoscopic scale.

Figure 4(a) shows that more dislocations nucleate near point D than point A. Accordingly, cleavage proceeds after dislocations emit, and the spread deformation field associated with a running crack suppresses the further dislocation emission. Only incomplete dislocations are observed near the cracking path, as indicated in Figure 4(b) by several slip traces in about 45° direction with respect to the crack.

The moiré fringes kink along these lines. These slip traces are nearly parallel to each other, suggesting that a crack propagated in step-by-step manner, as illustrated in Figure 6.

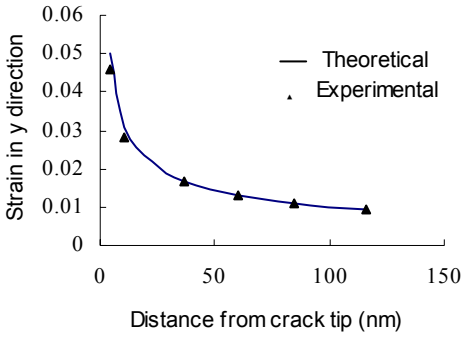

Figure 5 Strain distribution in *y* direction ahead of the crack tip.

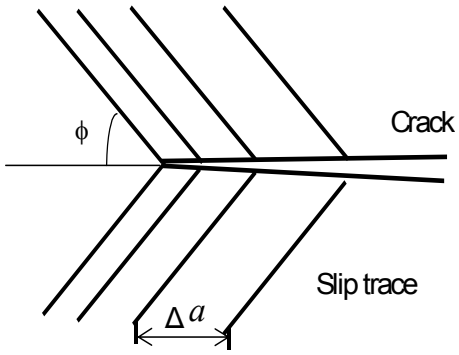

Figure 6 Schematics of crack growth in step-by-step manner

Zielinski *et al.* [10] reported step-by-step crack growth for Fe-2wt%Si and showed that the cleavage crack left 3.5 slip traces of residual dislocations for every 100nm crack growth, with an average of 18.6 dislocations per trace. Zhu *et al.* [11] defined a crack tip opening angle (CTOA) as $\mathrm{CTOA} = 2\tan^{-1}\left(nb\sin\phi/\Delta a\right)$, where b denotes the amplitude of Burgers vector, Δa the step size of cracking and n the number of dislocations emanated during each cracking step. In the present case, the incomplete dislocations has to be included as:

$$\mathrm{CTOA} = 2\tan^{-1}\left(\frac{nb+\delta_r}{\Delta a}\sin\phi\right) \qquad (3)$$

Where δ_r represents the slip in radial direction due to incomplete dislocations. The non-mismatched moiré fringes in Figure 4(a) can be used to determine the CTOA as $b/\Delta f$, where Δf is the fringe interval along AD nearest to the current crack tip. The CTOA is evaluated as $0.014\mathrm{rad}$. Near the current crack tip, no complete dislocation have been formed, thus one has $n = 0$. The measurement from Figure 4(b) gives $\phi \approx \pi/4$ and $\Delta a = 20\sim30\mathrm{nm}$. Equation (3) then estimates the value of δ_r from 0.2 to 0.3nm, less than the lattice spacing 0.304nm of silicon.

Two kinds of dislocations can be observed from the fringe pattern. Three complete dislocations, whose moiré fringes share the similar features with Figure 1, can be observed near the point D of Figure 4(a). The other kind is the incomplete or Peierls-dislocations, one of them is along the line *or* in Figure 4(b). The moiré fringes are sheared along this line. They represent slip between lattice layers. The amount of slip gradually changes along the line *or*, as recorded in Figure 7. The slip of lattice is zero at the point far from the crack tip and is one Burgers vector at the tip. This type of lattice slip assembles the structure of a nucleated Peierls dislocation [3] from a crack tip that provides direct experimental support for the Peierls framework concept [4].

The slip range represents the width of a dislocation. Based on the Frenkel sinusoidal shear stress-slip relation, Beltz and Rice estimated the width of a Peierls dislocation from a crack tip as $R = 0.0628Eb^2/[(1-\nu^2)\gamma_{us}]$, where γ_{us} denotes the unstable stacking energy [4]. For silicon, $\gamma_{us} = 0.16Eb$, consequently $R \approx 4.36b$. The present test, however, suggests a much larger value of

$R \approx 600b$, as evidenced in Figure 7. Explanation is needed for such a long extension of dislocation slip from a crack tip.

AKNOWLEGEMENT

The authors greatfully acknowledge the support by the National Natural Science Foundation of China (19962001).

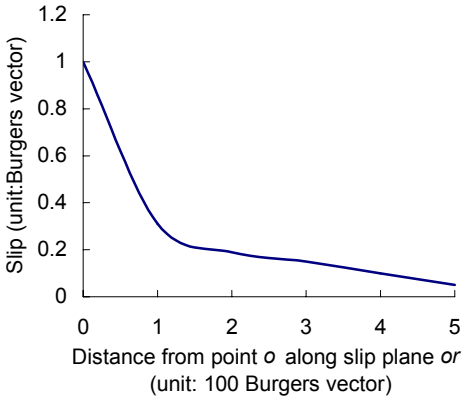

Figure 7 Slip distribution along a Peierls dislocation

REFERENCE

1. Ashby, M.F. and Embury(1985), J.D. Spripta Metall. 19, 557; Argon, A.S., Acta Metall(1987). 35, 185; Brede M. and Haasen, P.(1988) Acta Metall. 36, 2003; Hirsch, P.B. and Roberts, S.G. Phil. Mag. (1991) A64, 55; Hsia, K.J. and Argon, A.S. (1994), Mater. Sci. & Eng. A176, 111.
2. Rice, J.R. and Thomson, R.(1974), Phil. Mag., 29, 73.
3. Peierls R.E. (1940), Proc. Phys. Soc. 52, 23.
4. Argon, A.S.(1987), Acta Metall. 35, 185; Chiao,Y.H. and Clark, D.R.(1989) Acta Metall. 37, 203; Schoeck, G.(1991), Phil. Mag. A63, 111; Rice, J.R.(1992), J. Mech. Phys Solids 40, 239; Beltz G.E.and Rice, J.R. (1992), Acta Metall. Mater. 40, 321; Rice, J.R. and Beltz, G.E. (1994), J. Mech. Phys. Solids 42, 333; Schoeck, G. (1994), Phil. Mag. A69, 1085.
5. John, C.S., (1975),Phil. Mag. 32, 1193; Brede, M. K., Hsia J.and Argon, A.S., J.(1991)Appl. Phys. 70, 758; Mesarovic, S.D.J. (1997), J. Mech. Phys. Solids, 211.
6. Post, D.(1980), Mechanics of Nondestructive Testing, ed. Stinchcomb, W.W., Plenum Press, NY,; Kishimoto, S. *et al.*, Proceedings of 6th International Conference on Mechanical Behavior of Materials, ed. Jones(1991), M.,4, 661; Dally, J.W. and Read, D.T.(1993)., Experimental Mechanics 33, 2704
7. Dai, F.L and Xing, Y.M.(1999), Acta Mechanica Sinica 15, 283.
8. Hirsch, P., Howie, A., Nicholson, R., Pashley, D.W. and Whelan, M.J.(1977), Electron Microscopy of Thin Crystals, Krieger, Malabar, FL.
9. Mao T.H. *et al*(1983), J. Materials Sci. Letter, 2, 613; Shield T. W.and Kim, K.S. (1994), J. Mech. Phys. of Solids, 42, 845; Shi Y. Q., *et al.*(1996), Experimental Mechanics, 36, 193.
10. Zielinski, W., Lii, M.J.and Gerberich, W.W. (1992), Acta Metall. Mater. 40, 2861.
11. Zhu, T. Yang, W.and Guo, T. (1996), Acta Metall. Mater. 44, 3049.